IEEE Open Journal of
Antennas and Propagation

Received 20 February 2021; revised 13 March 2021; accepted 14 March 2021. Date of publication 19 March 2021; date of current version 2 April 2021.

Digital Object Identifier 10.1109/OJAP.2021.3067373

Optimized Differential TCDA (D-TCDA) With Novel Differential Feed Structure

ALEXANDER D. JOHNSON (Member, IEEE), VIGNESH MANOHAR (Member, IEEE), SATHEESH BOJJA VENKATAKRISHNAN (Member, IEEE), AND JOHN L. VOLAKIS (Fellow, IEEE)

Department of Electrical and Computer Engineering, College of Engineering and Computing, Florida International University, Miami, FL 33174, USA

CORRESPONDING AUTHOR: V. MANOHAR (e-mail: vmanohar@fiu.edu)

This work was supported by the Air Force Office of Scientific Research under Grant FA9550-19-1-0290.

ABSTRACT Modern phased arrays require large instantaneous bandwidths, wide fields of view, and low profiles to conduct multiple functions. Many of these phased arrays rely on emerging high speed ADCs and advanced balanced transceivers. The benefits of balanced front-ends include improved linearity, dynamic range, isolation, and noise resilience. The application of a differential phased array in such a system removes extraneous losses caused by baluns, though the issue of feed-borne E-plane scan resonances must be considered. We address the E-plane scan resonance issue through an improved Balanced Wideband Impedance Transformer (BWIT) feed for the ultra-wideband (UWB) Tightly Coupled Dipole Array (TCDA). This BWIT feed has already demonstrated mitigated common-modes over a 3:1 bandwidth ratio while scanning to low angles. Here, our differential TCDA (D-TCDA) is developed for the L-C band (*viz.* 1.0 GHz to 6.1 GHz) with emphasis on resonance-free wide-angle scanning. Rigorous EM model and circuit analysis is included to verify the BWIT performance. Under a VSWR < 3 definition, the improved array achieves a 6:1 impedance bandwidth ratio (BWR) with resonance-free scanning in all planes. An exception is the H-plane scanning at 60° where the VSWR < 4. Array simulations are verified with measurements for an 8×8 single-polarized prototype.

INDEX TERMS Antenna arrays, differential geometry, phased arrays, ultra-wideband antennas.

I. INTRODUCTION

MODERN phased arrays are required to be low volume, high gain, multifunctional, and capable of large fields of view [1]. It is well known that ultrawideband (UWB) systems are an enabler of multi-function operations through their wide access to the (radio frequency) RF spectrum. These federated systems also reduce cost, space, weight and power (C-SWaP) burdens that multiple systems would incur. In support of such multi-functional requirements, modern RF hardware is being developed with balanced (differential) components and interconnects [2]. These differential configurations enable the attributes needed for multifunction systems: high linearity, high dynamic range, and high isolation. Further, balanced transmission lines suppress distortions due to even order harmonics from nonlinear devices [3]. One missing system aspect is the proliferation of differentially fed antennas (e.g., dipoles or spirals) to directly connect to these balanced systems and remove extraneous baluns from the RF chain. The removal of these unnecessary balun stages, especially in the case of an UWB balun, significantly reduces associated losses and phase/amplitude mismatches.

Tightly Coupled Dipole Antenna (TCDA) arrays are a good candidate for such multifunctional systems, since they are inherently UWB and able to scan over much larger volumes than spiral arrays [4]. Recent optimization of TCDA resulted in 1) increased impedance bandwidths (BWR) greater than 46:1 [5], 2) low angle scanning down to 75° using Frequency Selective Surface (FSS) superstrates [6], [7], 3) low cost fabrication methods [8], [9], and 4) operation at millimeter-wave (mm-wave) frequencies [10].

Typical of all metal-backed planar dipole arrays, TCDAs require a well-matched balanced excitation at the dipole

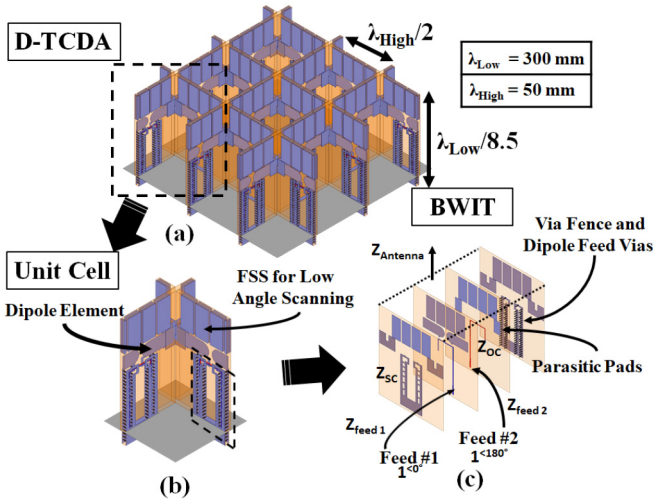

FIGURE 1. Pictorial representation of a (a) dual polarized differential TCDA (D-TCDA) array with (b) unit cell of dual offset D-TCDA design, along with the (c) improved BWIT differential matching network.

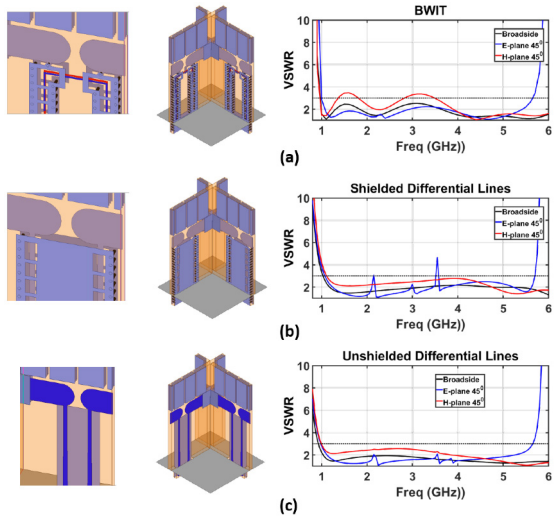

FIGURE 2. Impedance matching using various feeds: (a) BWIT, (b) shielded twin line, and (c) unshielded twin lines.

terminal, with a feed that extends a distance H above the ground plane, (where $\lambda/4 < H < \lambda/2$ at the matched bands shortest wavelength). Typical dipole antennas are fed by traditional differential (e.g., twin line) feeds. In an array setting, these also provide UWB broadside performance. However, they exhibit ruinous common-modes when implemented in a phased array that scans to low angles. The balanced antennas in [11], [12], [13], [14] all exposed the occurrence of common modes in their feeds, which caused efficiency-disastrous resonances. These common modes are present at frequencies and scan angles (typically mid-band and >45°) where mutual coupling between co-polarized array elements introduces a phase imbalance on the feed [15], [16]. Often, these feeds are perpendicular to the ground plane to incur image theory's aid at a distance H. These common-mode currents transition the feed from a transmission line to a radiating monopole structure, essentially pulling energy and efficiency from the aperture. It is for this reason that most TCDA designs include integrated balun (TCDA-IB) [17], which would require a second (and unnecessary) balun in the aforementioned balanced system configuration. Aside from simply using a balun feed, other work have investigated disrupting the coupled fields through conductive [8], [11], [12], [18], [19] or lossy means [13]–[14].

In this paper, we present a differential TCDA (D-TCDA) alternative to TCDA-IB that allows balanced feeding without common-mode resonances, complex coupling shields, or intentional losses. Here the presented D-TCDA in Fig. 1 builds on the works of [20], [21], [22] with an optimized version of the Balanced Wideband Impedance Transformer (BWIT) feed structure. In relation to the previous D-TCDA works, the presented array 1) operates at a higher frequency band with 2) improved impedance matching, 3) wider scan volumes and 4) larger measured BWR. Specifically, this paper builds [22] to a) double the usable BWR from 3:1 to 6:1, b) provide a rigorous analysis for the BWIT's common-mode mitigation, and c) achieve resonance-free E-plane scanning down to 75° from boresight. We remark that in reference to the aforementioned common-mode mitigation techniques [6], [7], [11], [12], [13], [14], [17], [19], [23], the BWIT provides an unparalleled C-SWaP performance. In short, this D-TCDA is printed on low-cost PCBs, without using additive processes, and with high efficiency. This paper presents simulated analysis of both dual-polarized and single-polarized design concepts, but only the latter was fabricated for demonstration. Simulations were verified with measurements of the fabricated 8 × 8 prototype.

The paper is organized as follows. Section II presents the challenges with common-mode resonances in vertical differential feed Lines. Section III describes the design of the BWIT feed structure. The dual-polarized and single-polarized D-TCDA design implementations are given in Section IV, for operation across 1.0 GHz to 6.1 GHz. Section V gives fabrication and measurement details for the demonstrator.

II. COMMON-MODE SCAN RESONANCES IN VERTICAL DIFFERENTIAL FEED LINES

As mentioned, common-modes can arise in vertical differential feed lines of PEC backed arrays at certain scan angles and frequencies. This occurs when mutual coupling between elements causes a phase change in one of the balanced feed lines, resulting in an unbalanced (common) mode between the two signal conductors. If these common-mode currents appear perpendicular to the ground plane they radiate monopole type fields. To validate this, the setup in Fig. 2 shows the active VSWR under broadside and 45° scan radiation using different feeds. The feeds considered are 1) BWIT, 2) shielded twin line, and 3) unshielded twin line.

Although the typical differential feeds in Fig. 2 appear well matched at broadside across the UWB, common-mode

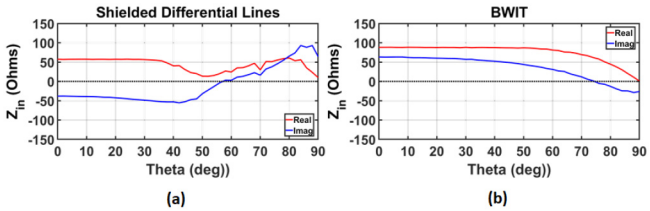

FIGURE 3. Infinite array simulations at the common mode resonant frequencies in Fig. 2 showing input impedance versus scan angle. Specifically (a) shielded twin lines at 3.6 GHz, and (b) BWIT feed at 2.2 GHz. The impedance values imply that the discontinuity in the shielded twin lines are a near-short at resonance and the BWIT is unaffected.

resonances in the E-plane are present for certain cases. For example, in the shielded differential lines of Fig. 2(b), there are resonances at 2.2 GHz, 3 GHz, and 3.6 GHz. There is also a small discontinuity in the BWIT VSWR, but this is a negligible mismatch. The sharp mismatches in the shielded differential lines refer to scan resonances that cause radiation from the vertically oriented differential transmission lines. This is further investigated by sweeping the scan angle and plotting the input impedance at the discontinuous frequencies found in Fig. 2. As depicted in Fig. 3, this study clearly shows that the twin line has a resonance (reactive zero crossing and practical RF short) at $45° < \theta < 60°$ at 3.6 GHz. The same shorting effect was first reported in [11]. The vector plots of the current distributions can be found in [20] and will not be repeated for brevity. Meanwhile, the BWIT shows good impedance matching out to the $\theta = 90°$ (horizon) and negligible mismatch impact at 2.2 GHz. Therefore, it can be concluded from these full-wave simulations that the BWIT feed is common-mode resilient when scanning. The following section gives insight into how this is achieved.

III. BALANCED WIDEBAND IMPEDANCE TRANSFORMER

As discussed above, many previous TCDA were fed by integrated Marchand baluns [17] with the characteristics of that in Fig. 4(a). The circuit model of this feed network includes a tapered feed, series open stub (Z_{oc}) and a parallel short stub (Z_{sc}). Using the circuit in Fig. 4(c), broadband matching is achieved through proper tuning of these variables, along with the height and coupling of the dipole. Since 2016, tapered ground conductor perforations were introduced in to the balun design [6], [24] to transform the 50 Ω input port to the 188 Ω [25] at the dipole feed without reverting to the previous split-cell approach [17].

By contrast, the D-TCDA presented here are instead excited by the BWIT feed network in Fig. 4(b). This balanced wideband impedance transformer consists of two coupled Marchand balun sections, as illustrated by the circuit diagram in Fig. 4(d). The real portion of the input impedance is controlled by the feed line's taper and perforated ground shield, using design rules from [6]. The BWIT also contains a pair of mirrored reactive transmission line components, X_{Stubs}. Each of these reactive transmission line components mirror the operation of a Marchand balun, with a series open stub and a parallel short stub, whose impedance and lengths

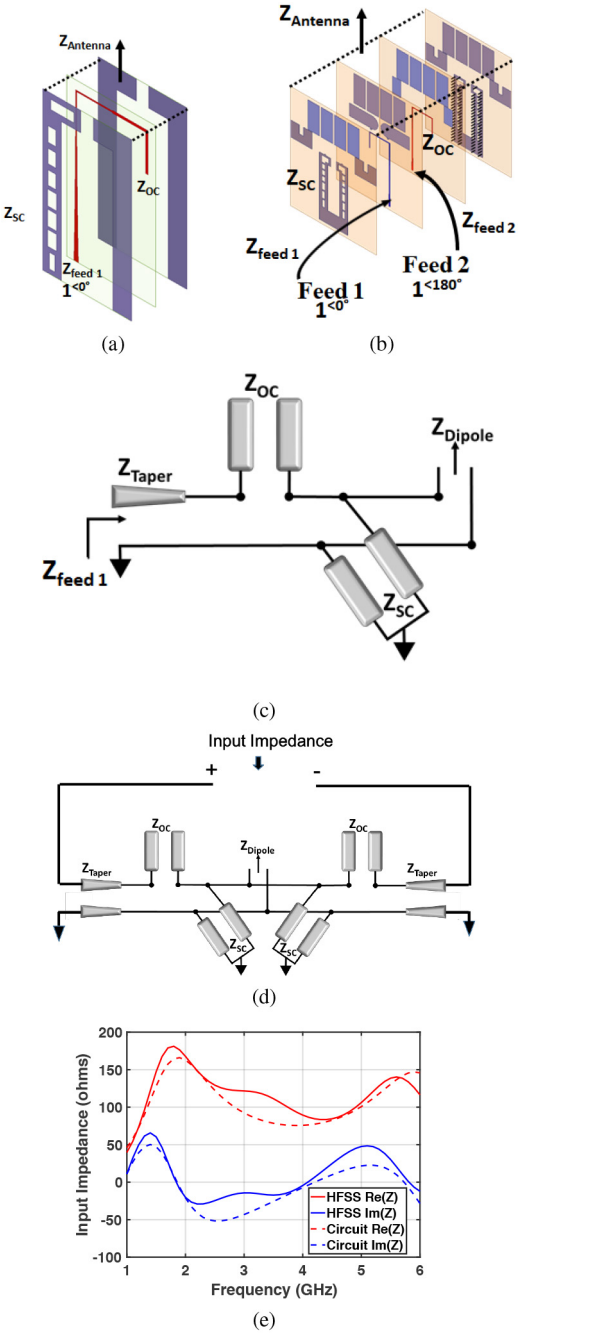

FIGURE 4. Marchand baluns for TCDAs: (a) Marchand balun sketch, (b) BWIT sketch, (c) behavioral circuit model, (d) BWIT behavioral circuit model, (e) BWIT impedance profile. The behavioral model is verified by its close relation to the full-wave impedance profile.

are tuned to achieve a broadband reactive match. The feed ensures balanced signal transmission from the feed to the aperture, with the help of the reactive components (X_{Stubs}) for scan cases.

To reiterate, both the circuit models in Figs. 4(c) and 4(d) are tuned for 1) UWB matching and 2) to suppress common-mode currents across large bandwidths across all scan angles. While the Marchand balun was already verified in [17], it serves as a template case for the BWIT circuit verification.

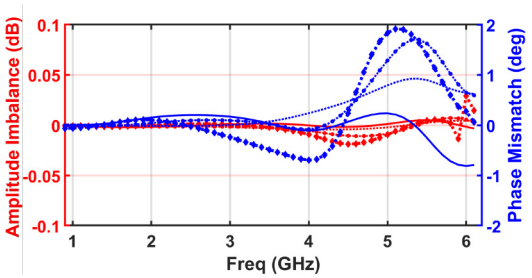

FIGURE 5. Amplitude variation and phase imbalance of the BWIT feed for broadside (solid) 45° (dashed), 60° (circle-dashed), and 75° (diamond-dashed) scanning cases.

Thus, using the same approach, Fig. 4(e) validates the behavioral circuit model of the BWIT feed using full wave HFSS simulations. Notably, the circuit model uses ideal transmission lines, with the square gabs on the outer conductive surfaces represented as an impedance tapered line [6] (see component $Z_{feed\ 1}$ in Fig. 4). The overall D-TCDA can be optimized quickly using this model in traditional circuit software, then verified by more time-consuming full-wave analysis.

The standalone BWIT feed was also simulated as an infinite array using ANSYS HFSS v.19 across the E-plane scan volume to determine its inherent common-mode-rejection ratio (CMRR). Here the TCDA aperture was simply represented by 188 Ω loads [25] and periodic boundary conditions defined the scan angle of the incoming wave. The BWIT exhibited low amplitude and phase imbalances (see Fig. 5) with insignificant common-mode influence over the scan volume. For the broadside case, the maximum amplitude variation was ±0.01 dB and with maximum phase imbalance of ±0.81 degrees. As shown, common-modes are mitigated, as only an additional ($< 2°$) phase imbalance is present in the 45°, 60°, and 75° scanning cases. Thus, the BWIT retains a CMRR >27 dB (see [26, Fig. 2]), with maximum amplitude balance of ±0.03 dB and maximum phase imbalance $< \pm 1.92°$ at the worst case of 75° scanning. The average insertion loss of this full-wave model was 0.69 dB, 0.92 dB, 1.03 dB and 0.99 dB across the band for scanning cases of 0°, 45°, 60°, and 75°, respectively.

To further demonstrate the resilience of BWIT feeds, we consider the equivalent circuits of three feeds: 1) typical twin line differential feed, 2) a Marchand balun, and 3) BWIT feed, as shown in Fig. 6. A phase mismatch (equivalent common-mode) was added to each of these feed lines to demonstrate common-mode resilience. Specifically, a 7° offset was added on a single leg of each feed at the furthest point from the Z_{Dipole} terminal (denoted by the arrows in Fig. 6). Fig. 6(a) shows that the common mode in the twin line circuit leads to multiple detrimental resonances across the band. However, the Marchand balun in Fig. 6(b) shows only an impedance change without resonances across the entire band (common-mode elimination). As shown, the reactive component, X_{Stubs}, is the discriminator between the differential line and Marchand balun fields for common-modes. This reactive network is also used in the BWIT

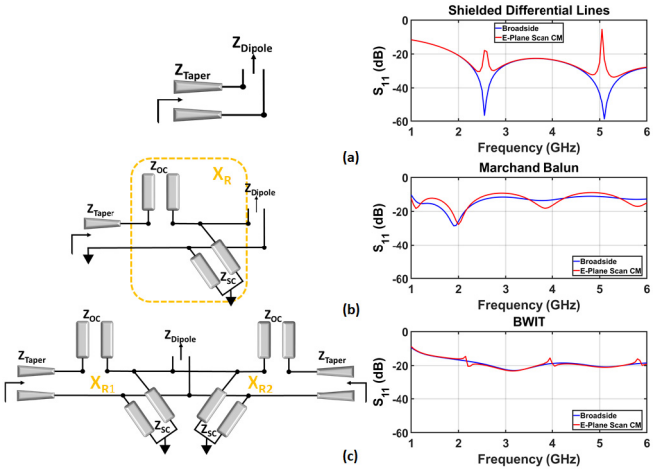

FIGURE 6. Transmission line equivalent circuits and S_{11} performance for three different feeds: (a) Basic differential lines, (b) Marchand Balun and (c) BWIT at broadside (red) and with a common mode excitation (blue).

feed (as a balanced pair) to mitigate common mode effects. Importantly, the BWIT feed with common mode excitation in Fig. 6(c) shows only minor impedance discontinuities. In fact, Fig. 3 shows these do not impact scan performance. That is, full-wave and circuit analysis show that the reactive aspect of the BWIT is a common-mode mitigator. Given these observations, the BWIT feed can be integrated into a fully differential TCDA (D-TCDA) to suppress common mode resonances and improve matching.

IV. TIGHTLY COUPLED DIPOLE ELEMENT DESIGN

The presented D-TCDA unit cell employs half-wave dipoles with capacitive overlaps as in previous TCDA. As depicted in Fig. 1(c), a 0.30 mm (12 mil) metal via connects the dipole arms on the center layer. This serves to feed the outer layers in a similar fashion to a Marchand balun. Also, a metal FSS superstrate is employed for wide-angle scanning [6], [24]. Specifically, sub-wavelength metallic rectangles are periodically printed above the dipoles to produce an effective dielectric constant, ϵ_{eff}, and remove the need for a thick dielectric slab above the D-TCDA. As in [22], parasitic layers were included at the ends of the dipoles to increase capacitive coupling and improve low frequency performance. However, in contrast, the dipoles are printed on the same layer as the FSS (see Layer 2 in Fig. 7). It is worth noting that capacitive coupling is a controllable variable to trade between lower frequency cutoffs (larger BWR) and maximum mismatch at the lower end of the matched band. That is, additional capacitive coupling can introduce sharp resonances to push a low frequency ground resonance downward, but this sharp reactance also increases the VSWR at the remaining lower portion of the matched band.

A. DUAL-POLARIZED DIFFERENTIALLY FED TCDA SIMULATIONS

Periodic unit cell (infinite array) simulations were used to emulate the performance of an embedded element of an

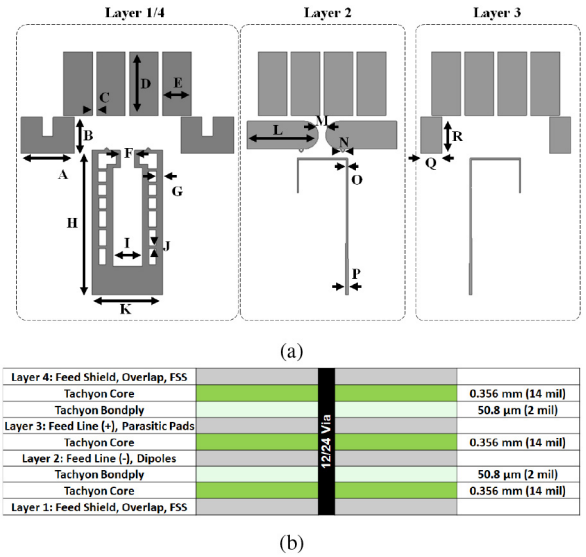

FIGURE 7. (a) Unit cell details of the designed dual-polarized D-TCDA. The (b) antenna stack-up shows the mirrored metal layers are printed on 0.36mm (14 mil) substrate layers with relative dielectric constant of $\varepsilon_r = 3.0$.

TABLE 1. Dimensions (units : mm) of dual-polarized D-TCDA in Fig. 7.

A	B	C	D	E	F	G	H	I
7.66	5.27	0.60	9.20	4.14	2.00	0.93	20.85	4.18
J	**K**	**L**	**M**	**N**	**O**	**P**	**Q**	**R**
0.38	10.18	10.24	1.00	0.61	0.25	0.45	3.03	5.27

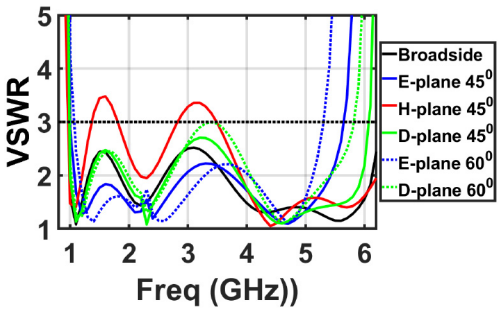

FIGURE 8. Simulated infinite array VSWR in the E, H, and D-planes of the dual-polarized array at broadside and scanning to 60° in the E/D-planes and 45° in the H-plane.

electrically large array. Here the D-TCDA is excited as a differential system through the BWIT feed, which can be represented as the balanced port [27] in Fig. 4(b). Fig. 8 shows the infinite array active VSWR of the dual-polarized design in Fig. 1, with resonant-free scanning down to 60°. In this case, the array provides a broadside VSWR < 2.5 across 1.0-6.1 GHz, implying an impedance bandwidth of 6.1:1. Typical with low profile planar arrays [7], [19], the H-plane scanning VSWR degrades at lower frequencies. Notably, the inclusion of additional superstrate matching layers have shown improved H-plane VSWR [19], though this translates to an increased aperture height. The dimensions

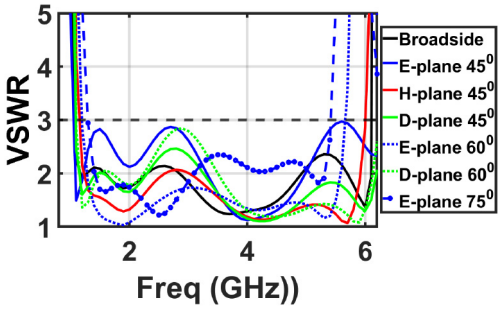

FIGURE 9. Simulated infinite array VSWR in the E, H, and D-planes of the single-polarized array. Broadside and scanning VSWR at 45° and 60° are shown.

of the dual-polarized design in Fig. 1 are given in Fig. 7 and Table 1.

B. SINGLE-POLARIZED DIFFERENTIALLY FED TCDA

Although the above mentioned D-TCDA shows promising full-wave results, a single polarized array was also designed for a reduced cost demonstrator. This design shares the same PCB stackup and basic design features (i.e., BWIT feed, capacitive overlap, and FSS superstrate) as the dual-polarized version. Infinite array simulations of this single-polarized D-TCDA also used 100Ω characteristic impedance balanced excitiations [27]. Fig. 9 shows the single polarized array's VSWR in the principle (E/H) and diagonal planes (D-plane), demonstrating resonant-free scanning to 60°. The single-polarized D-TCDA variant provides a broadside VSWR $<$ 2.5 across 1.05-6.15 GHz, implying an impedance bandwidth of 5.85:1. This slight reduction in BWR from the dual-polarized variant is expected since the present edge capacitance is reduced. Below we present measured data for this single polarized array.

V. D-TCDA PROTOTYPE FABRICATION AND MEASUREMENTS

A. D-TCDA PROTOTYPE FABRICATION

The 8×8 single-polarized D-TCDA prototype (Fig.10) was fabricated for design verification. The PCB based D-TCDA consists of three 0.36 mm (14 mil) Isola Tachyon ($\epsilon_r = 3.0$, $\tan\delta = 0.0021$) laminates, with a metal tolerance of 0.25 mm (10 mil) and dimensions as shown in Fig. 11 and Table 2. Note that this 8×8 array has four identical center elements, and one of them was chosen to be the embedded element for measurements. Low profile edge mount SMPM connectors were used to feed the array. The 22.86cm$\times$22.86cm ground board in Fig. 10 was milled from a metalized 1.52mm (60 mil) FR4 board with element profile cutouts for mounting. Styrofoam blocks $\epsilon_r = 1.1$ were also used for alignment and mechanical supports under the ground plane. This setup forms a large, lightweight structure that is stable and resonance free for testing and evaluation.

B. D-TCDA MEASUREMENTS

For S-parameter measurements, a 4-port Vector Network Analyzer (VNA) was employed in an internally calibrated

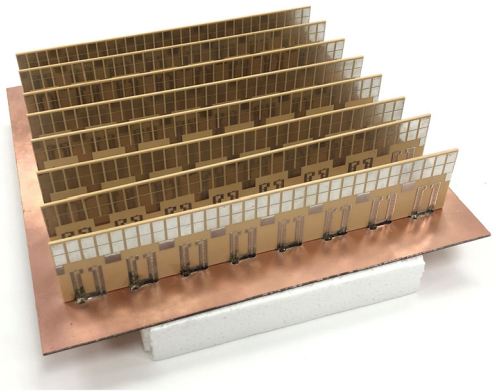

FIGURE 10. Fabricated 8×8 single-polarized D-TCDA placed on a 22.86cm×22.86cm ground plane.

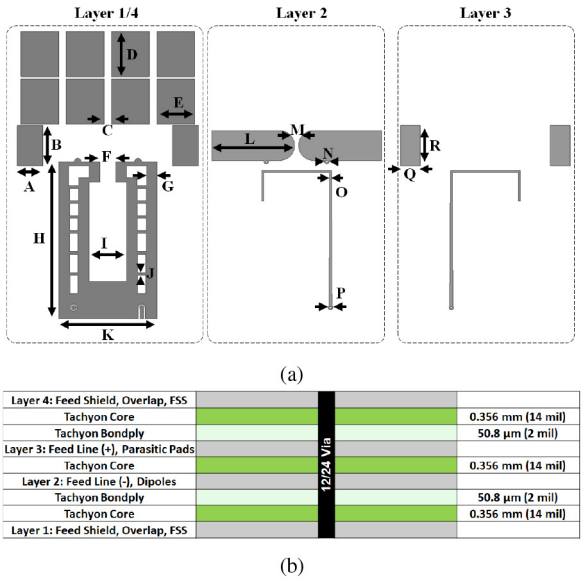

FIGURE 11. (a) Unit cell details of the fabricated single-polarized D-TCDA. The (b) antenna stack-up shows the mirrored metal layers are printed on 0.36 mm (14 mil) substrate layers with relative dielectric constant of $\varepsilon_r = 3.0$.

TABLE 2. Dimensions (units: mm) of single-polarized D-TCDA in Fig. 11.

A	B	C	D	E	F	G	H	I
3.43	5.33	1.00	6.00	5.00	2.09	1.40	20.85	5.00
J	**K**	**L**	**M**	**N**	**O**	**P**	**Q**	**R**
0.38	13.0	11.0	0.51	0.61	0.25	0.61	2.62	5.30

differential mode. Specifically, two ports (e.g., ports 1 and 2) were used to serve as an ideal 180° hybrid coupler to measure the balanced S-parameters for each dipole. A 20.32 cm (8.0") SMPM-SMA cable [28] was also used with standard SMA ports on the VNA for measurements. Notably, due to lack of SMPM calibration resources, the calibration reference plane was the SMA interface of the SMA-SMPM cable.

The active balanced VSWR of a center embedded element was measured and extracted by adding the balanced reflection coefficient S_{nn} of the center element to the balanced coupling terms from the surrounding elements S_{nm}.

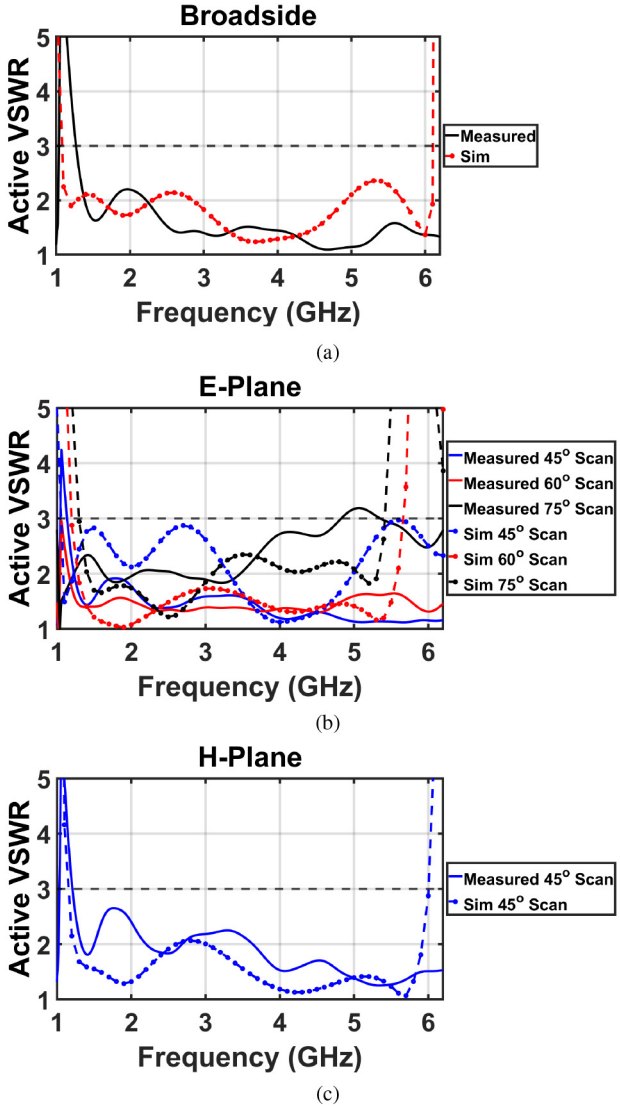

FIGURE 12. Measured active VSWR of the center embedded element for (a) broadside, (b) E-Plane, and (c) H-Plane cases with comparison to simulations, showing resonant free scanning down to 75° in the E-plane.

During the measurements, the remaining element's differential ports, (two SMPM per element) were each terminated in 50Ω matched loads. The measured active VSWR of a center embedded element is depicted in Fig. 12 along with semi-finite simulations. As seen, the measured active VSWR yields an almost 6:1 impedance bandwidth with VSWR $<$ 3 from 1.15 GHz to 6.2 GHz for all scan cases, except the measured 75° E-plane scan. Notably, the lower cutoff frequency of the measured VSWR is slightly higher due to fabrication tolerances and the inclusion of the SMPM-SMA cables. We further remark that as is the case for all finite TCDA, the outer element performance will be degraded as compared to the center embedded element due to edge effects. These edge effects primarily impact the lower frequencies, since the element's capacitance is insufficient to cancel the ground plane inductance. Notably, this edge element performance impact has been discussed in previous

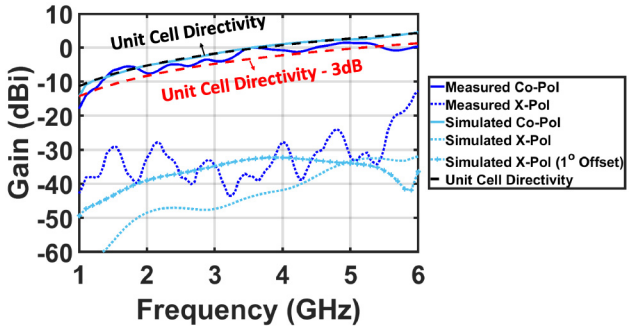

FIGURE 13. Measured vs simulated co-polarized and cross-polarized gain of the center embedded element as a function of frequency. Measurements show >30 dB cross-polarization purity across the band.

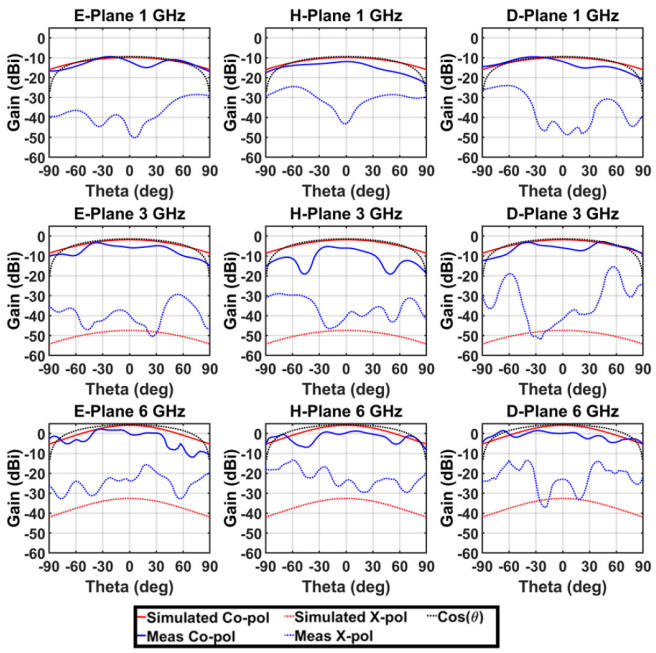

FIGURE 14. Measured vs simulated embedded patterns of the center element in the E-plane at 1 GHz, 3 GHz, and 6 GHz. More than 20 dB polarization purity is achieved out to $\theta = \pm 60°$.

TCDA publications [5], [22], [24], and is not repeated here for brevity.

The embedded center element gain was measured with the aid of an external UWB balun [29], to comply with the testing chamber's single-ended equipment. This balun was de-embedded in post-processing. As noted, the SMA-SMPM cable's effect was included in the measurements. Fig. 13 shows the measured broadside co-polarized and cross-polarized gain for the embedded center element with comparisons to simulations. Also, Fig. 14 shows the center element patterns in the E/H/D Planes indicating 20 dB cross-polarization purity down to $\theta = 60°$. Notably, the measured patterns closely follow the predicted values and the cos θ pattern reference. The apparent differences between the simulated and measured cross-polarized gain levels are due to small physical misalignments in the setup [30]. Such impact is depicted in Fig. 13 for $\phi = 1°$ misalignment in the antenna aperture plane. As can be seen, $\phi = 1°$ misalignment can greatly increase the perceived cross-polarized gain levels. Notably, the proposed antenna is constructed using low-loss PCB substrates ($\tan\delta = 0.0021$). The simulated radiation efficiency for our unit cell was $> 95\%$ over the entire band. As noted, this paper follows past works by showing measured data for only an embedded element [19], [22], [24]. The gain of the finite array is ultimately determined by the size of the array and number of active elements.

VI. CONCLUSION

An improved L-C band (*viz.* (1.0 GHz to 6.1 GHz) differentially-fed TCDA (D-TCDA) was presented. The paper's emphasis was on achieving wide-angle resonance-free scanning for single and dual-linear polarized D-TCDA configurations. A key contribution of the paper is the novel Balanced Wideband Impedance Transformer (BWIT) feed that mitigated common-mode resonances when scanning to low angles across large bandwidths. Rigorous full-wave and circuit analysis is provided to show the benefits of the BWIT over standard twin-line balanced array feeds.

A behavioral model of the proposed wideband differential feed was validated and used to optimize the antenna's performance. Specifically, an 8×8 single-polarized D-TCDA was fabricated and measured. Measurements showed good agreement with simulations. In summary, when used in conjunction with differential RF components, this array 1) removes extraneous baluns in the chain, and 2) enables high dynamic range, high linearity, and low noise differential radio receivers.

REFERENCES

[1] A. D. Johnson, B. McMahon, M. Livadaru, and M. Fosberry, "Phased array advantages at BAE systems," in *Proc. IEEE 63rd Int. Midwest Symp. Circuits Syst. (MWSCAS)*, Springfield, MA, USA, 2020, pp. 428–431.

[2] *Zynq UltraScale+ RFSoC*. [Online]. Available: https://www.xilinx.com/support/documentation/datasheets/ds889-zynq-usp-rfsoc-overview.pdf.

[3] D. M. Pozar, "Microwave engineering education: From field theory to circuit theory," in *IEEE/MTT-S Int. Microw. Symp. Dig.*, Montreal, QC, Canada, Jun. 2012, pp. 1–3.

[4] I. Tzanidis, K. Sertel, and J. L. Volakis, "Interwoven spiral array (ISPA) with a 10:1 Bandwidth on a ground plane," *IEEE Antennas Wireless Propag. Lett.*, vol. 10, pp. 115–118, 2011.

[5] A. D. Johnson, J. Zhong, S. B. Venkatakrishnan, E. A. Alwan, and J. L. Volakis, "Phased array with low-angle scanning and 46:1 bandwidth," *IEEE Trans. Antennas Propag.*, vol. 68, no. 12, pp. 7833–7841, Dec. 2020.

[6] E. Yetisir, N. Ghalichechian, and J. L. Volakis, "Ultrawideband array with 70° scanning using FSS superstrate," *IEEE Trans. Antennas Propag.*, vol. 64, no. 10, pp. 4256–4265, Oct. 2016.

[7] A. O. Bah, P.-Y. Qin, R. W. Ziolkowski, Y. J. Guo, and T. S. Bird, "A wideband low-profile tightly coupled antenna array with a very high figure of merit," *IEEE Trans. Antennas Propag.*, vol. 67, no. 4, pp. 2332–2343, Apr. 2019.

[8] M. W. Elsallal, J. R. Hood, and R. Kindt, "Development of substrate-free frequency-scaled ultra-wide spectrum element (FUSE) phased array," in *Proc. IEEE Int. Symp. Phased Array Syst. Technol. (PAST)*, Waltham, MA, USA, Oct. 2016, pp. 1–5.

[9] M. R. Naeini, M. Mirmozafari, and D. van der Weide, "Monolithic 3-D printing of an integrated marchand balun with a dipole antenna," *IEEE Trans. Compon., Packag. Manuf. Technol.*, vol. 10, no. 4, pp. 654–658, Apr. 2020.

[10] M. H. Novak, F. A. Miranda, and J. L. Volakis, "Ultra-wideband phased array for millimeter-wave ISM and 5G bands, realized in PCB," *IEEE Trans. Antenns Propag.*, vol. 66, no. 12, pp. 6930–6938, Dec. 2018.
[11] J.-P. R. Bayard, D. H. Schaubert, and M. E. Cooley, "E-plane scan performance of infinite arrays of dipoles printed on protruding dielectric substrates: Coplanar feed line and E-plane metallic wall effects," *IEEE Trans. Antennas Propag.*, vol. 41, no. 6, pp. 837–841, Jun. 1993.
[12] S. Edelberg and A. Oliner, "Mutual coupling effects in large antenna arrays II: Compensation effects," *IRE Trans. Antennas Propag.*, vol. 8, no. 4, pp. 360–367, Jul. 1960.
[13] J. J. Lee, S. Livingston, and R. Koenig, "Performance of a Wideband (3-14 GHz) Dual-pol Array," in *Proc. IEEE Antennas Propag. Soc, Symp.*, vol. 1. Monterey, CA, USA, Jun. 2004, pp. 551–554.
[14] E. de Lera Acedo, E. Garcia, V. González-Posadas, J. L. Vazquez-Roy, R. Maaskant, and D. Segovia, "Study and design of a differentially-fed tapered slot antenna array," *IEEE Trans. Antennas Propag.*, vol. 58, no. 1, pp. 68–78, Jan. 2010.
[15] S. G. Hay and J. D. O'Sullivan, "Analysis of common-mode effects in a dual-polarized planar connected-array antenna," *Radio Science*, vol. 43, p. RS6S04, Dec. 2008.
[16] D. Cavallo, A. Neto, and G. Gerini, "PCB slot based transformers to avoid common-mode resonances in connected arrays of dipoles," *IEEE Trans. Antennas Propag.*, vol. 58, no. 8, pp. 2767–2771, Aug. 2010.
[17] J. P. Doane, K. Sertel, and J. L. Volakis, "A wideband, wide scanning tightly coupled dipole array with integrated balun (TCDA-IB)," *IEEE Trans. Antennas Propag.*, vol. 61, no. 9, pp. 4538–4548, Sep. 2013.
[18] A. D. Johnson, S. B. Venkatakrishnan, E. A. Alwan, and J. L. Volakis, "Suppressing E-plane scan resonance for UWB millimeter-wave differential phased array," in *Proc. Int. Appl. Comput. Electromagn. Soc. Symp. (ACES)*, Miami, FL, USA, Apr. 2019, pp. 1–2.
[19] J. T. Logan, R. W. Kindt, M. Y. Lee, and M. N. Vouvakis, "A new class of planar ultrawideband modular antenna arrays with improved bandwidth," *IEEE Trans. Antennas Propag.*, vol. 66, no. 2, pp. 692–701, Feb. 2018.
[20] A. D. Johnson, S. B. Venkatakrishnan, E. A. Alwan, and J. L. Volakis, "Balanced wideband impedance transformer (bwit) for common-mode resonance cancellation in uwb dipoles over a ground plane," in *Proc. Int. Appl. Comput. Electromagn. Soc. Symp. (ACES)*, Monterey, CA, USA, 2020, pp. 1–2.
[21] A. Johnson, "Ultra-wideband phased arrays for small mobile platforms," Ph.D. dissertation, Dept. Elect. Eng., Florida Int. Univ., Miami, FL, USA, 2019.
[22] A. D. Johnson, J. Zhong, M. Livadaru, S. B. Venkatakrishnan, E. A. Alwan, and J. L. Volakis, "Wideband dipole array with balanced wideband impedance transformer (bwit)," *IEEE Open J. Antennas Propag.*, vol. 2, pp. 163–169, 2021.
[23] W. Elsallal, J. Hood, A. Locker, and R. Kindt, "Frequency-scaled ultra-wide spectrum element," U.S. Patent 9 991 605B2, 2019.
[24] J. Zhong, A. Johnson, E. A. Alwan, and J. L. Volakis, "Dual-linear polarized phased array with 9:1 Bandwidth and 60° scanning off broadside," *IEEE Trans. Antennas Propag.*, vol. 67, no. 3, pp. 1996–2001, Mar. 2019.
[25] E. A. Alwan, K. Sertel, and J. L. Volakis, "Circuit model based optimization of ultra-wideband arrays," in *Proc. IEEE Int. Symp. Antennas Propag.*, Chicago, IL, USA, Jul. 2012, pp. 1–2.
[26] D. Jorgesen and C. Marki, *Balun Basics Primer*. Morgan Hill, CA, USA: Marki Microw., 2015, pp. 1–3.
[27] D. E. Bockelman and W. R. Eisenstadt, "Combined differential and common-mode scattering parameters: Theory and simulation," *IEEE Trans. Microw. Theory Techn.*, vol. 43, no. 7, pp. 1530–1539, Jul. 1995.
[28] *Cable Assembly Coaxial SMA to SMP*. Accessed: Mar. 15, 2021. [Online]. Available: https://www.digikey.com/product-detail/en/amphenol-rf/095-902-459-008/ARF2558-ND/6559768
[29] *Bal0010*. Accessed: Mar. 15, 2021. [Online]. Available: https://www.markimicrowave.com/baluns/bal-0010.aspx
[30] A. Ludwig, "The definition of cross polarization," *IEEE Trans. Antennas Propag.*, vol. 21, no. 1, pp. 116–119, Jan. 1973.

ALEXANDER D. JOHNSON (Member, IEEE) received the B.S. degree in electrical engineering from Western New England University, Springfield, MA, USA, in 2016, the M.S. degree in electrical engineering from The Ohio State University, Columbus, OH, USA, in 2017, and the Ph.D. degree in electrical and computer engineering from Florida International University (FIU), Miami, FL, USA, in 2019.

From August 2019 to September 2020, he worked as a Research Assistant Professor with FIU. He is currently a Principal Scientist with BAE Systems, Merrimack, NH, USA. His research interests include novel materials, textile electronics, wideband array apertures, mm-wave phased arrays, and simultaneous transmit and receive systems. He was a NASA Research Announcement Fellowship Award recipient in 2018. He also received an Honorable Mention in the Student Paper Competition at the 2019 IEEE Antenna and Propagation Symposium (AP-S/URSI), and the Student Fellowship Travel Grant Award at the U.S. National Committee for the International Union of Radio Science (USNC–URSI) in 2017 and 2018.

VIGNESH MANOHAR (Member, IEEE) received the bachelor's degree in electronics and telecommunication engineering from the University of Mumbai in 2013, and the M.S. and Ph.D. degrees in electrical and computer engineering from the University of California, Los Angeles, Los Angeles, CA, USA, in 2016 and 2020, respectively.

He is currently a Postdoctoral Associate with the Department of Electrical and Computer Engineering, Florida International University. His research area focuses on the development of wideband antenna arrays, and deployable high gain aperture antennas for small satellite platforms. He was a recipient of the Outstanding Masters Thesis Award in the Physical and Wave Electronics for the year 2016 and the Henry Samueli Excellence in Teaching Award in 2020. He received an Honorable Mention in the 2017 and 2018 Altair FEKO Student Competition for his work on stepped reflectors and characterizaition of planar near-field antenna measurements respectively. He was also a recipient of the 2019 IEEE Electromagnetic Theory Symposium Young Scientist Award for his work on umbrella reflector antenna characterization.

SATHEESH BOJJA VENKATAKRISHNAN (Member, IEEE) was born in Tiruchirappalli, India, in 1987. He received the bachelor's degree in electronics and communication engineering from the National Institute of Technology, Tiruchirappalli, in 2009, and the M.S. and Ph.D. degrees in electrical engineering from the Ohio State University (OSU), Columbus, OH, USA, in 2017.

He was a Scientist for DRDO, India, from 2009 to 2013, working on the development and implementation of active electronic steerable antennas. He is currently a Research Assistant Professor of Electrical and Computer Engineering with Florida International University. His current research includes receiver design for communication circuits, RF systems, and digital signal processing using FPGAs. He is also working on simultaneous transmit and receive system, to improve the spectral efficiency. He was an IEEE Electromagnetic Theory Symposium (EMTS-2019) Young Scientist Award recipient. He won the Second Prize in International Union of Radio Science General Assembly and Scientific Symposium student paper competition held at Montreal, Canada, in August 2017. He also received Honorable Mention in the student paper competition at the IEEE Antenna and Propagation Symposium (AP-S/URSI) in 2015 and 2016, and the Student Fellowship Travel Grant Award at the U.S. National Committee for the International Union of Radio Science (USNC–URSI) in 2016 and 2017. He has been a Phi Kappa Phi Member since 2015.

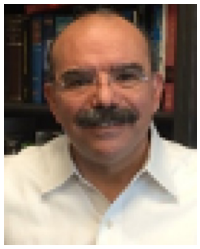

JOHN L. VOLAKIS (Fellow, IEEE) was born on May 13, 1956, in Chios, Greece and immigrated to the U.S.A. in 1973. He received the B.E. degree *(summa cum laude)* from Youngstown State University, Youngstown, OH, USA, in 1978, and the M.Sc. and Ph.D. degrees from The Ohio State University, Columbus, OH, USA, in 1979 and 1982, respectively.

He started his career with Rockwell International (currently Boeing) from 1982 to 1984. In 1984, he was appointed as an Assistant Professor with The University of Michigan, Ann Arbor, MI, USA, becoming a Full Professor in 1994. He also served as the Director of the Radiation Laboratory from 1998 to 2000. From January 2003 to August 2017, he was the Roy and Lois Chope Chair Professor of Engineering with the Ohio State University and served as the Director of the ElectroScience Laboratory from 2003 to 2016. Since August 2017, he has been the Dean of the College of Engineering and Computing and a Professor in the Electrical and Computer Engineering at Florida International University (FIU). He has graduated/mentored 95 doctoral students/postdoctorals with 43 of them receiving best paper awards at conferences. His publications include eight books, 430 journal papers, nearly 900 conference papers, 29 book chapters and 25 patents/disclosures. His coauthored books are: *Approximate Boundary Conditions in Electromagnetics*, 1995; *Finite Element Methods for Electromagnetics*, 1998; *Antenna Engineering Handbook*, (4th ed., 2007); *Small Antennas*, 2010; and *Integral Equation Methods for Electromagnetics*, 2011. Over the years, he carried out research in antennas, wireless communications and propagation, computational methods, electromagnetic compatibility and interference, design optimization, RF materials, multiphysics engineering, millimeter waves, terahertz and medical sensing. Among his awards are: The University of Michigan College of Engineering Research Excellence Award in 1993, the Scott Award from The Ohio State University College of Engineering for Outstanding Academic Achievement in 2011, the IEEE AP Society C.-T. Tai Teaching Excellence Award in 2011, the IEEE Henning Mentoring Award in 2013, the IEEE Antennas and Propagation Distinguished Achievement Award in 2014, The Ohio State University Distinguished Scholar Award in 2016, The Ohio State University ElectroScience George Sinclair Award in 2017, and the URSI Booker Gold Medal in 2020. His service to Professional Societies include: the President of the IEEE Antennas and Propagation Society (2004), the Chair of USNC/URSI Commission B (2015–2017), twice the General Chair of the IEEE Antennas and Propagation Symposium, IEEE APS Distinguished Lecturer, IEEE APS Fellows Committee Chair, IEEE-Wide Fellows Committee Member, and an associate editor of several journals. He was listed by ISI among the top 250 most referenced authors in 2004, and is a Fellow of ACES and URSI.